PRAMANA
— journal of
physics

Vol. 85, No. 4
October 2015
pp. 639–651

On the role of deformed Coulomb potential in fusion using energy density formalism

LAVNEET KAUR and RAJ KUMARI*

Department of Physics, Panjab University, Chandigarh 160 014, India
*Corresponding author. E-mail: rajkumari80pu@gmail.com

MS received 28 January 2014; revised 12 July 2014; accepted 28 July 2014
DOI: 10.1007/s12043-014-0898-z; ***e*Publication:** 29 January 2015

Abstract. Using the Skyrme energy density formalism, the effect of deformed Coulomb potential on fusion barriers and fusion cross-sections is studied. Our detailed study reveals that the fusion barriers as well as fusion probabilities depend on the shape deformation (due to deformed Coulomb potential) of the colliding nuclei. However, this dependence due to deformed Coulomb potential is found to be very weak.

Keywords. Fusion probabilities; quadrupole deformation; Skyrme energy density formalism.

PACS Nos 24.10.−i; 25.60.Pj; 25.70.−z

1. Introduction

With the advent of advanced accelerators and sophisticated detectors, the study of nuclear reactions has come a long way. The study of heavy-ion collisions gives the possibility to examine nuclear interaction in the form of ion–ion potential as well as fusion at low incident energies and in the form of multifragmentation [1,2], nuclear flow [3] etc., at intermediate incident energies. At energies close or below the Coulomb barrier, the interaction time between the colliding nuclei is large and therefore, various features of a nucleus such as its shape, surface vibrations and neutron transfer, which do not play any important role at higher incident energies, are dominating factors at below barrier energies.

At low incident energies, many potentials are available to calculate the nuclear part of the interaction potential such as proximity-based potential models [4]. Among the various proximity-based models, the Skyrme energy density formalism (SEDF) [5,6] takes into account the spin-orbit dependent part which involves the structural effects of the colliding nuclei. It also takes into account Skyrme interactions that represent the effective nuclear force valid for low relative momenta cases. The Skyrme force is a phenomenological nuclear force first proposed by Skyrme [7]. This force is zero range and is

density-dependent in nature. This force consists of a two-body term V_{ij} and a three-body term V_{ijk}.

$$V = \sum_{i<j} V_{ij}^{(2)} + \sum_{i<j<k} V_{ijk}^{(3)}. \tag{1}$$

The three-body term describes the way in which interactions between two nucleons are influenced by the presence of a third nucleon. The Skyrme force has a few adjustable parameters t_0, t_1, t_2, t_3 and W_0, the values of which can be adjusted for better description of various ground-state properties such as binding energies, nucleon densities, root mean square (rms) radii of nuclei, etc.

As far as Coulomb part of the interaction potential is concerned, a very few efforts have been made to modify it [8]. In these studies, different models (double-folding model, quantum-diffusion approach) were used to obtain approximate expressions for the Coulomb potential between two deformed nuclei. In another study by Manhas *et al* [9], the effect of adding quadrupole deformations β_2 and higher multipole deformation (β_3, β_4, β_6, and β_8) on distribution of barriers for spherical deformed and deformed–deformed nuclei was studied using generalized fragmentation theory. We find that such studies were not conducted yet, using Skyrme energy density formalism. Motivated by [9], we aim to study the effect of deformed Coulomb potential on fusion barrier heights as well as the fusion probabilities using SEDF. Our study is confined to quadrupole deformation β_2, because it was clearly mentioned in [9] that β_3 is known to be nonzero for only a few nuclei, β_6 is insignificant for collisions involving deformed–deformed systems and β_8 is significant for collisions involving spherical deformed systems. Since, in the present study, we deal with spherical deformed as well as deformed–deformed systems, we restrict our study to quadrupole deformation.

For this study, the nuclear part of the nucleus–nucleus interaction potential is assumed to be independent of deformation. The deformation enters the Coulomb potential through the deformation parameter β_2, which describes the collective behaviour of a nucleus. For spherically symmetric nucleus, $\beta_2 = 0$, i.e., $b = a$, where a and b represent semimajor and semiminor axes, respectively. In a prolate deformed nucleus, $\beta_2 > 0$, i.e., $b > a$, and so the matter is distributed along the angular momentum axis. In oblate-deformed nucleus $\beta_2 < 0$, i.e., $b < a$, and so there is a flattened distribution of matter about the angular momentum axis. In the present work, we aim to study the role of oblate and prolate quadrupole deformations in Coulomb potential of the colliding nuclei on fusion probabilities using different Skyrme forces. Here, we shall use Skyrme forces S, SIII, SV and SKa. The choice of these Skyrme forces is based on the idea that the Skyrme force S has no density dependence whereas force SIII has density dependence. The Skyrme force SIII is widely used to study the heavy-ion potential at low incident energies because this force is found to reproduce most of the experimental data on binding energies and rms radii. For the force SV, $t_3 = 0$, and so this is simply a two-body force with no density dependence. The total interaction potential calculated using Skyrme forces from S to SVI show similar trend, i.e., these remain attractive at larger distances and become repulsive at shorter distances. On the other hand, the Skyrme force SKa remains attractive throughout.

This paper is organized as follows. Section 2 gives a brief description of the model and §3 gives the results and discussions. Finally, summary is presented in §4.

2. The model

The nuclear potential $V_N(R)$ is defined as the difference between the energy expectation value E of the two colliding nuclei at a finite distance R and at infinity [5,6,10]:

$$V_{\mathrm{N}}(R) = E(R) - E(\infty). \tag{2}$$

The energy E at infinity represents the binding energy of a nucleus in isolation. The energy expectation value E is given by

$$E = \int H(\vec{r})\mathrm{d}\vec{r}. \tag{3}$$

The energy density functional $H(\vec{r})$ associated with Skyrme interaction is given by

$$\begin{aligned} H(\vec{r}) = {} & \frac{\hbar^2\tau}{2m} + \frac{t_0}{2}\left[\left(1+\frac{x_0}{2}\right)\rho^2 - \left(x_0+\frac{1}{2}\right)\left(\rho_{\mathrm{n}}^2+\rho_{\mathrm{p}}^2\right)\right] + \frac{1}{4}(t_1+t_2)\rho\tau \\ & + \frac{1}{8}(t_2-t_1)(\rho_{\mathrm{n}}\tau_{\mathrm{n}}+\rho_{\mathrm{p}}\tau_{\mathrm{p}}) + \frac{1}{16}(t_2-3t_1)\rho\nabla^2\rho \\ & + \frac{1}{32}(3t_1+t_2)(\rho_{\mathrm{n}}\nabla^2\rho_{\mathrm{n}}+\rho_{\mathrm{p}}\nabla^2\rho_{\mathrm{p}}) + \frac{1}{16}(t_1-t_2)(\vec{J}_{\mathrm{n}}^2+\vec{J}_{\mathrm{p}}^2) \\ & + \frac{1}{4}t_3\rho_{\mathrm{n}}\rho_{\mathrm{p}}\rho - \frac{1}{2}W_0(\rho\vec{\nabla}\cdot\vec{J}+\rho_{\mathrm{n}}\vec{\nabla}\cdot\vec{J}_{\mathrm{n}}+\rho_{\mathrm{p}}\vec{\nabla}\cdot\vec{J}_{\mathrm{p}}), \end{aligned} \tag{4}$$

with $\rho = \rho_{\mathrm{n}} + \rho_{\mathrm{p}}$, $\tau = \tau_{\mathrm{n}} + \tau_{\mathrm{p}}$ and $\vec{J} = \vec{J}_{\mathrm{n}} + \vec{J}_{\mathrm{p}}$. The quantities ρ, τ and $\vec{J}$ are nucleon density, kinetic energy density and spin density, respectively. The subscripts n and p refer to neutron and proton respectively. The different Skyrme force parameters t_0, x_0, t_1, t_2, t_3 and W_0 are fitted by different physicists to obtain various ground-state properties. The interaction potential becomes

$$V_{\mathrm{N}}(R) = \int \left[H(\rho,\tau,\vec{J}) - \{H_1(\rho_1,\tau,\vec{J}_1) - H_2(\rho_2,\tau,\vec{J}_2)\}\right]\mathrm{d}\vec{r}. \tag{5}$$

One can divide the Hamiltonian into two parts involving the spin-independent and spin-dependent parts [6]

$$V_{\mathrm{N}}(R) = V_{\mathrm{P}}(R) + V_{\mathrm{J}}(R), \tag{6}$$

where $V_{\mathrm{P}}(R)$ is the spin density independent part and $V_{\mathrm{J}}(R)$ is the spin density dependent part.

The spin-independent part $V_{\mathrm{P}}(R)$ can be calculated in accordance with the proximity theorem. The proximity theorem states that the force between gently curved surfaces as a function of the separation degree of freedom s is proportional to the interaction potential per unit area, $e(s)$, between two flat surfaces; the proportionality factor being 2π times the reciprocal of the square root of the Gaussian curvature of the gap width function at the

point of closest approach [11]. According to the theorem, the nuclear proximity potential, $V_{\rm P}(R)$, of the two spherical nuclei, with radii C_1 and C_2 and whose centres are separated by a distance $R = s + C_1 + C_2$, is given by

$$\begin{aligned} V_{\rm P}(R) &= \int [H(\rho) - \{H_1(\rho_1) - H_2(\rho_2)\}]{\rm d}\vec{r} \\ &= 2\pi \bar{R}\Phi(s), \end{aligned} \tag{7}$$

where $\Phi(s)$ is a universal function and is given by

$$\Phi(s) = \int \{H(\rho) - [H_1(\rho_1) + H_2(\rho_2)]\}{\rm d}Z, \tag{8}$$

and mean curvature radius $\bar{R}$ is given by

$$\bar{R} = \frac{C_1 C_2}{C_1 + C_2}\,, \tag{9}$$

with the Süssmann central radii C_i, expressed in terms of equivalent spherical nuclear radii R_i as

$$C_i = R_i - \frac{b}{R_i}, \tag{10}$$

where $R_i = 1.28A_i^{1/3} - 0.76 + 0.8A_i^{-1/3}$ given by Blocki [11] and surface diffuseness $b \approx 1$ fm.

The spin-dependent part can be further simplified as

$$\begin{aligned} V_{\rm J}(R) &= \int [H(J) - \{H(J_1) + H(J_2)\}]{\rm d}\vec{r} \\ &= -\frac{W_0}{2}\int [\rho_1 \vec{\nabla}\cdot\vec{J}_2 + \rho_2\vec{\nabla}\cdot\vec{J}_1 + \rho_{\rm n1}\vec{\nabla}\cdot\vec{J}_{\rm n2} + \rho_{\rm n2}\vec{\nabla}\cdot\vec{J}_{\rm n1} \\ &\quad + \rho_{\rm p1}\vec{\nabla}\cdot\vec{J}_{\rm p2} + \rho_{\rm p2}\vec{\nabla}\cdot\vec{J}_{\rm p1}]{\rm d}\vec{r} \end{aligned} \tag{11}$$

which under the assumption $\rho_{\rm n1} = \rho_{\rm p1} = \frac{1}{2}\rho_1$ becomes

$$V_{\rm J}(R) = -\frac{3}{4}W_0 \int [\rho_2\vec{\nabla}\cdot(\vec{J}_{\rm n1} + \vec{J}_{\rm p1}) + \rho_1\vec{\nabla}\cdot(\vec{J}_{\rm n2} + \vec{J}_{\rm p2})]{\rm d}\vec{r}. \tag{12}$$

The spin density $\vec{J}(\vec{r})$ can be divided into core and valence particles as

$$\vec{J}(\vec{r}) = \vec{J}_{\rm c}(\vec{r}) \pm \vec{J}_{{\rm n}\nu}(\vec{r}). \tag{13}$$

The first term gives the contribution owing to the core consisting of closed shells and second term represents the valence particles (holes) n_ν; with + for particles and − for holes. The contribution of the core and hole in terms of shells can be written as

$$\vec{J}_{\rm c}(\vec{r}) = \frac{\vec{r}}{4\pi r^4}\sum_\alpha (2j_\alpha + 1)\Big[(j_\alpha(j_\alpha+1) - l_\alpha(l_\alpha+1) - \frac{3}{4}\Big]R_\alpha^2(\vec{r}), \tag{14}$$

$$\vec{J_{n\nu}}(\vec{r}) = \frac{n_\nu \vec{r}}{4\pi r^4}\Big[j(j+1) - l(l+1) - \frac{3}{4}\Big]R_l^2(\vec{r}), \tag{15}$$

where $R_{nl}(r)$ is the normalized radial wave function which reads as

$$R_{nl}(\vec{r}) = C_{nl} r^{l+1} \mathrm{e}^{-\nu r^2} v_{nl}(2\nu r^2) \tag{16}$$

with

$$C_{nl} = \Big[\frac{[2^{l-n+2}(2\nu)^{l+(3/2)}(2l+2n+1)!!]}{\sqrt{\pi}[(2l+1)!!]^2 n!}\Big]^{1/2}$$

and

$$v_{nl}(x) = \sum_{k=0}^{n} (-1)^k 2^k \binom{n}{k} \frac{(2l+1)!!}{(2l+2k+1)!!} x^k,$$

where the scaling factor ν is given by

$$2\nu = \frac{41 A^{-1/3} mc^2}{\hbar^2 c^2} \text{ (in fm}^{-2}\text{)}. \tag{17}$$

The nucleon densities used in the formalism is given by

$$\rho_i(r_i) = \rho_{0i}\Big[1 + \exp\left(\frac{r_i - R_{0i}}{a_i}\right)\Big]^{-1}, \tag{18}$$

where R_{0i} is the half density radii, which gives the distance from the centre at which the density is reduced to half of its maximum value and a_i is the surface diffuseness parameter, which is defined as the distance over which the density drops from 90% to 10% of its maximum value ρ_0. For further detailed explanation of Skyrme energy density model, one can refer to [6]. Using eqs (7) and (11), the nuclear part of the interaction potential $V_{\mathrm{N}}(R)$ can be calculated.

The barrier formation occurs due to complex interplay between the nuclear and Coulomb potentials as [5,6]

$$V_{\mathrm{T}}(R) = V_{\mathrm{N}}(R) + V_{\mathrm{C}}(R). \tag{19}$$

The expression for the Coulomb interaction $V_{\mathrm{C}}(R)$ between the two deformed colliding nuclei as given in [12] is

$$V_{\mathrm{C}}(R,\theta) = \frac{Z_1 Z_2 e^2}{R} + \sqrt{\frac{9}{20\pi}} \frac{Z_1 Z_2 e^2}{R^3} \sum_{i=1}^{2} R_i^2 \beta_{2i} P_2(\cos\theta_i)$$

$$+ \frac{3}{7\pi} \frac{Z_1 Z_2 e^2}{R^3} \sum_{i=1}^{2} R_i^2 [(\beta_{2i} P_2(\cos\theta_i)]^2, \tag{20}$$

where θ_i is the angle between the radius vector $\vec{R}$ and the symmetry axis of the ith nucleus, R_i is the effective sharp radius of the ith nucleus and parameter β_{2i} corresponds to the quadruple deformation of the ith nucleus.

During the collision, the two interacting nuclei may have many possible orientations (θ_1, θ_2). Therefore, it is preferred to take average over all the possible relative orientations (0° to 180°) of two deformed colliding nuclei while studying the fusion between them. We restrict to the condition that both the colliding nuclei are in the same plane (i.e., $\phi = 0$). Therefore, the Coulomb potential calculated above is independent of the angle ϕ. It is known that the quadruple deformation (β_2) and higher-order deformations (β_3, β_4) etc., satisfy the relation $\beta_2^2 \approx \beta_{l\geq 3}$. Therefore, terms which are linear and quadratic in quadruple deformation of nuclei are considered and the terms including higher-order deformations are neglected [12]. The values of quadruple deformation parameter (β_{2i}) for this study are taken from [13].

Once the total interaction potential $V_{\mathrm{T}}(R)$ is calculated, the barrier height V_{B} and barrier position R_{B} can be extracted as

$$\left.\frac{\mathrm{d}V_{\mathrm{T}}(R)}{\mathrm{d}R}\right|_{R=R_{\mathrm{B}}} = 0, \quad \left.\frac{\mathrm{d}^2V_{\mathrm{T}}(R)}{\mathrm{d}R^2}\right|_{R=R_{\mathrm{B}}} \leq 0. \tag{21}$$

Once the barrier positions and heights are known, one can calculate the fusion cross-section. The extensively used formula for the fusion cross-section is due to Wong [14]. In this, it was assumed that the absorption into the fusion channels takes place due to tunnelling through the barrier. For energies corresponding to a trajectory close and below the barrier top, the barrier looks like an inverted parabola. The expression for the same is given as

$$V_{\mathrm{T}}(R) = V_{\mathrm{N}}(R) + V_{\mathrm{C}}(R) = V_{\mathrm{B}} - \frac{1}{2}\mu^2\omega^2(R - R_{\mathrm{B}})^2. \tag{22}$$

Here, μ and ω are the reduced mass of the fusing system and the frequency of the oscillator, respectively. The probability of penetration at the top of this inverted harmonic-oscillator potential is one-half. Therefore, the interaction barrier for the lth partial wave is defined as the energy E_l at which the absorption probability is one-half. The interaction barrier for the s-wave is known as the Coulomb barrier. In the Wong model, this Coulomb barrier was measured by employing a simple analytic expression for the total reaction cross-section taken from the ingoing-wave strong-absorption model [15].

In Wong formalism, the cross-section for a complete fusion $\sigma_{\mathrm{fus}}(E_{\mathrm{c.m.}})$ is given by

$$\sigma_{\mathrm{fus}}(E_{\mathrm{c.m.}}) = \frac{\pi}{k^2}\sum_{l=0}^{l_{\max}}(2l+1)T_l(E_{\mathrm{c.m.}}), \tag{23}$$

where $k = \sqrt{2\mu E_{\mathrm{c.m.}}/\hbar^2}$ and $l_{\max}$ corresponds to the largest partial wave for which a pocket still exists in the interaction potential and $T_l(E_{\mathrm{c.m.}})$ is the energy-dependent

barrier penetration factor, approximated by Hill–Wheeler formula for a parabolic interaction barrier [16] as

$$T_l(E_{\text{c.m.}}) = \left[1 + \exp\left\{\frac{2\pi}{\hbar\omega_l}(V_{\text{B}}^l - E_{\text{c.m.}})\right\}\right]^{-1}, \tag{24}$$

where $V_{\text{B}}^l(R_{\text{B}}^l)$ and $\hbar\omega_l$ are the barrier height and curvature, respectively, for the lth partial wave. The above-mentioned Hill–Wheeler expression is valid only in the proximity of the barrier (i.e., at energy slightly above and below the Coulomb barrier). R_{B}^l and $\hbar\omega_l$ are insensitive to l and therefore, given by

$$R_{\text{B}}^l \simeq R_{\text{B}}^0, \quad \hbar\omega_l \simeq \hbar\omega_0 \tag{25}$$

and

$$V_{\text{B}}^l \cong V_{\text{B}}^0 + \frac{\hbar^2 l(l+1)}{2\mu(R_{\text{B}}^0)^2}. \tag{26}$$

Using the above assumptions and replacing the summation in eq. (23) by an integral, and taking $(l + \frac{1}{2})^2 = \chi$, we get

$$\sigma_{\text{fus}}(E_{\text{c.m.}}) = \frac{2\pi}{k^2}\int_{1/4}^{\chi} \text{d}\chi \left[\frac{1}{1 + \exp\{\frac{2\pi}{\hbar\omega_0}(V_{\text{B}}^0 + \frac{\hbar^2 l(l+1)}{2\mu(R_{\text{B}}^0)^2} - E_{\text{c.m.}})\}}\right], \tag{27}$$

which reduces to

$$\sigma_{\text{fus}}(\text{mb}) = 10\frac{(R_{\text{B}}^0)^2\hbar\omega_0}{2E_{\text{c.m.}}} \ln\left[1 + \exp\left\{\frac{2\pi}{\hbar\omega_0}(E_{\text{c.m.}} - V_{\text{B}}^0)\right\}\right]. \tag{28}$$

3. Results and discussions

In this study, the fusion barriers and fusion probabilities for the reactions ^{30}Si+^{62}Ni, ^{58}Ni+^{74}Ge, ^{30}Si+^{24}Mg, ^{40}Ca+^{96}Zr, ^{28}Si+^{62}Ni, ^{64}Ni+^{74}Ge, ^{16}O+^{76}Ge and ^{16}O+^{92}Zr are calculated. These reactions are grouped under different categories like spherical–oblate (S+O), spherical–prolate (S+P), oblate–oblate (O+O) and prolate–prolate (P+P) depending upon the value of the deformation parameter used for colliding nuclei in deformed Coulomb potential.

In table 1, values of various Skyrme parameters for Skyrme forces S, SIII, SV and SKa are displayed and in tables 2 and 3, the barrier heights calculated using these forces

Table 1. The Skyrme force parameters currently in use.

Skyrme force	t_0 (MeV fm^3)	t_1 (MeV fm^5)	t_2 (MeV fm^5)	t_3 (MeV fm^6)	W_0 (MeV fm^5)
S	−1072.00	461.00	−40.00	8027.00	0.00
SIII	−1128.75	395.00	−95.00	14000.00	120.00
SV	−1248.29	970.56	107.22	0.00	150.00
SKa	−1602.78	570.88	−67.70	8000.00	125.00

Table 2. Fusion barrier heights V_B (MeV) calculated using SEDF for Skyrme force S and SIII are displayed for the reactions of spherical colliding nuclei as well as deformed colliding nuclei (by including deformation up to β_2). These barrier heights are calculated from the total interaction potential averaged over all possible relative orientations θ_i (0° to 180°) of two deformed colliding nuclei. The corresponding empirical values are also listed.

Category	Reaction	Z_1Z_2	S V_B (MeV)	S Def V_B (MeV)	SIII V_B (MeV)	SIII Def V_B (MeV)	Empirical V_B (MeV)	Ref.
S+O	^{30}Si + ^{62}Ni	392	51.17	51.08	51.51	51.42	52.20 ±0.9	[18]
							52.10	[21]
S+O	^{58}Ni + ^{74}Ge	896	109.10	108.62	110.01	109.51	107.5	[19]
S+P	^{30}Si + ^{24}Mg	168	24.00	24.02	24.14	24.17	24.80	[17]
S+P	^{40}Ca + ^{96}Zr	800	98.66	99.23	98.90	99.48	94.59	[20]
O+O	^{28}Si + ^{62}Ni	392	51.66	51.24	52.06	51.62	52.89	[18]
							51.30	[21]
O+O	^{64}Ni + ^{74}Ge	896	107.51	106.84	108.18	107.48	105.1	[19]
P+P	^{16}O + ^{76}Ge	256	35.24	35.37	35.37	35.50	35.00	[22]
P+P	^{16}O + ^{92}Zr	320	43.29	43.36	43.44	43.51	41.96	[23]

are displayed for the above-mentioned reactions along with the experimental data. It is clear from the table that the barrier heights decrease for S+O and O+O cases and increase for the case of S+P and P+P compared to the spherical–spherical case. This may be due to the reason that in the case of oblate-deformed nucleus, two of the axes are major and one is minor. However, in the case of prolate-deformed nucleus, only one axis is major and two axes are minor. Therefore, the probability of overlapping along

Table 3. Fusion barrier heights V_B (MeV) using SEDF for Skyrme forces SV and SKa. The corresponding empirical values are also listed.

Category	Reaction	Z_1Z_2	SV V_B (MeV)	SV Def V_B (MeV)	SKa V_B (MeV)	SKa Def V_B (MeV)	Empirical V_B (MeV)	Ref.
S+O	^{30}Si + ^{62}Ni	392	49.85	49.76	48.86	48.77	52.20 ±0.9	[18]
							52.10	[21]
S+O	^{58}Ni + ^{74}Ge	896	106.41	105.96	104.34	103.91	107.5	[19]
S+P	^{30}Si + ^{24}Mg	168	23.31	23.34	22.84	22.88	24.80	[17]
S+P	^{40}Ca + ^{96}Zr	800	95.87	96.40	94.22	94.72	94.59	[20]
O+O	^{28}Si + ^{62}Ni	392	50.32	49.93	49.22	48.86	52.89	[18]
							51.30	[21]
O+O	^{64}Ni + ^{74}Ge	896	104.85	104.21	102.93	102.33	105.1	[19]
P+P	^{16}O + ^{76}Ge	256	34.24	34.36	33.93	34.05	35.00	[22]
P+P	^{16}O + ^{92}Zr	320	42.07	42.14	41.68	41.75	41.96	[23]

one major axis in prolate-deformed nucleus is less compared to that along two major axes in oblate-deformed nucleus. The barrier positions do not show any change on including deformation in Coulomb potential except for only few reactions.

In figure 1, we display total interaction potential V_T (MeV) as a function of internuclear distance R (fm) for ^{58}Ni+^{74}Ge, ^{40}Ca+^{96}Zr, ^{64}Ni+^{74}Ge and ^{16}O+^{76}Ge reactions under the category of S+O, S+P, O+O and P+P, respectively. In this figure, solid lines correspond to the total interaction potential calculated using Skyrme energy density formalism (SEDF) for the Skyrme forces S (light magenta), SIII (green), SV (black) and SKa (orange) by assuming the colliding nuclei to be spherical (i.e., $\beta_{21} = \beta_{22} = 0$). On the other hand, dashed coloured lines represent the total interaction potential for the same Skyrme forces, but now taking into consideration the deformed Coulomb potential of the colliding nuclei. The values of the deformation factor β_{2i} are taken from the experimental data. Figure 1 shows that Skyrme forces S, SIII and SV exhibit switching behaviour, i.e., they are first attractive and at smaller distances they become repulsive, whereas SKa force remains attractive throughout the distance. Also the depth of the fusion pocket is maximum for SV force but it is minimum for SIII force.

In figures 1a and 1b, the projectile is spherical, but the target is oblate and prolate deformed, respectively. In figure 1c, the colliding nuclei are of oblate–oblate combination whereas in figure 1d, the colliding nuclei are of prolate–prolate combination. Figure 1 shows that the total interaction potential gets modified by adding deformation to the Coulomb potential. In figures 1a and 1c, it is noticed that the fusion pocket becomes deeper for the fusion of S+O and O+O colliding nuclei than for the S+S reaction. On

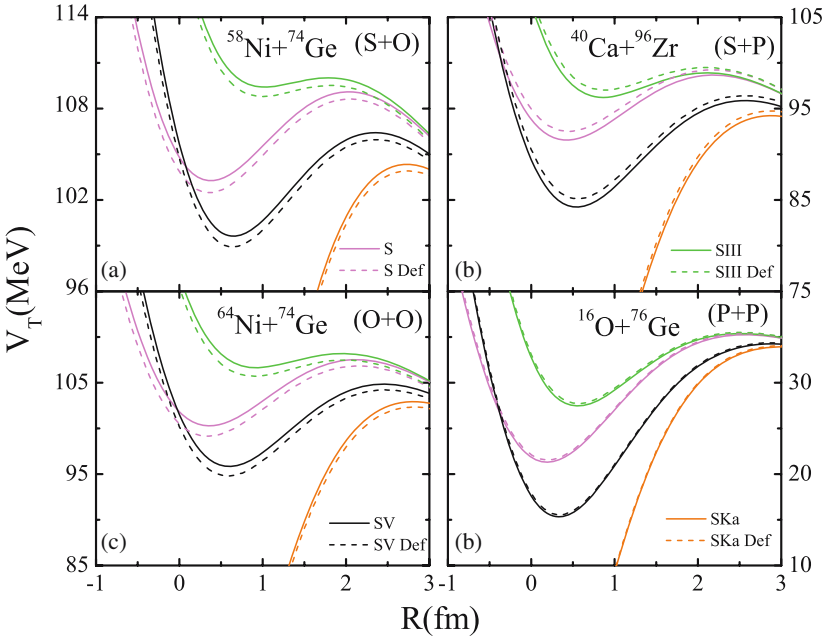

Figure 1. Total interaction potential V_T (MeV) as a function of internuclear distance R (fm) for the reactions (**a**) ^{58}Ni+^{74}Ge (S+O), (**b**) ^{40}Ca+^{96}Zr (S+P), (**c**) ^{64}Ni+^{74}Ge (O+O) and (**d**) ^{16}O+^{76}Ge (P+P). Various lines are explained in the text.

the other hand, in figures 1b and 1d, the fusion pocket becomes shallower for the S+P and P+P cases compared to the S+S case.

In figures 2–5, fusion cross-section σ_{fus} (mb) is displayed as a function of the centre-of-mass energy $E_{\text{c.m.}}$ (MeV). Various lines have same meaning as in figure 1. Figure 2 shows that the fusion probability is slightly more for the S+O nuclei than for the S+S case because the depth of the fusion well increases on adding deformation (S+O) as discussed earlier. So, for ^{30}Si+^{62}Ni and ^{58}Ni+^{74}Ge, the fusion probabilities increase for S+O combination of colliding nuclei at sub-barrier energies. In figure 3, it is seen that there is a decrease in the fusion probability for S+P case than for the S+S case. This is because the depth of the fusion well decreases on adding deformation. Therefore, in ^{30}Si+^{24}Mg and ^{40}Ca+^{96}Zr, the fusion probability decreases for S+P-deformed nuclei at sub-barrier energies. In figure 4 also, the same trend is observed as in figure 2, but it is seen that fusion probability is even more for the O+O combination than for the S+O case. So, fusion probability increases for oblate–oblate-deformed nuclei at sub-barrier energies. In figure 5, similar trend is observed as reported in figure 3. In this case, fusion probability decreases for prolate–prolate-deformed nuclei at sub-barrier energies, but this decrease is not noticeable due to the lack of experimental data for P+P (highly deformed) systems.

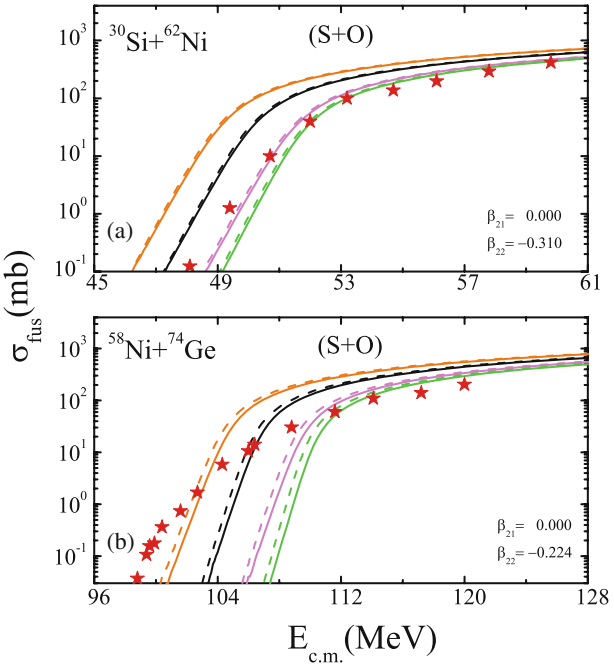

Figure 2. The fusion cross-section σ_{fus} (mb) as a function of the centre of mass energy $E_{\text{c.m.}}$ (MeV) for the reactions (**a**) ^{30}Si+^{62}Ni and (**b**) ^{58}Ni+^{74}Ge. In both (**a**) and (**b**), projectile is spherical and target is oblate-deformed. The experimental data for the ^{30}Si+^{62}Ni and ^{58}Ni+^{74}Ge reactions are taken from Stefanini *et al* [18] and Beckerman *et al* [19], respectively. Various lines imply the same meaning as in figure 1.

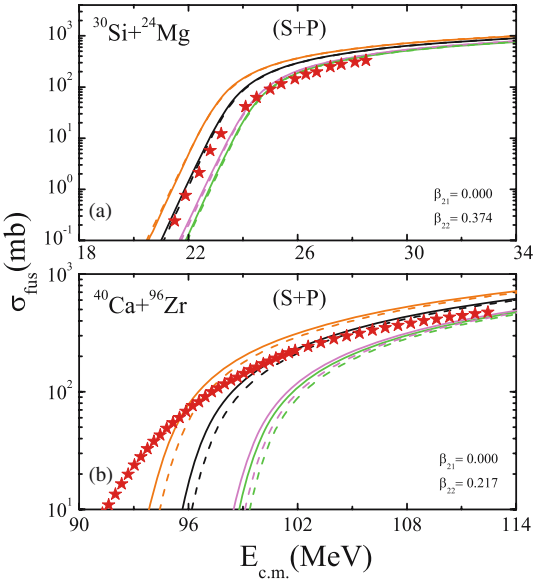

Figure 3. Same as figure 2, but for (**a**) ^{30}Si+^{24}Mg and (**b**) ^{40}Ca+^{96}Zr reactions. In both (**a**) and (**b**), projectile is spherical and target is prolate-deformed. The experimental data for these reactions are taken from Morsad *et al* [17] and Timmers *et al* [20], respectively.

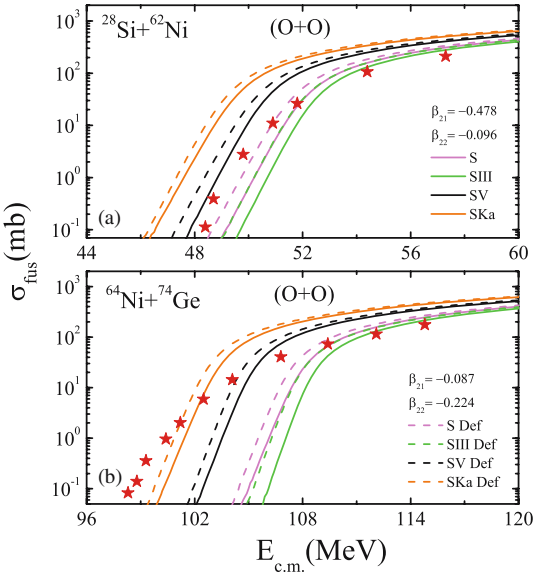

Figure 4. Same as figure 2, but for (**a**) ^{28}Si+^{62}Ni and (**b**) ^{64}Ni+^{74}Ge reactions. In both (**a**) and (**b**), projectile and target are oblate-deformed. The experimental data for these reactions are taken from Stefanini *et al* [18] and Beckerman *et al* [19], respectively.

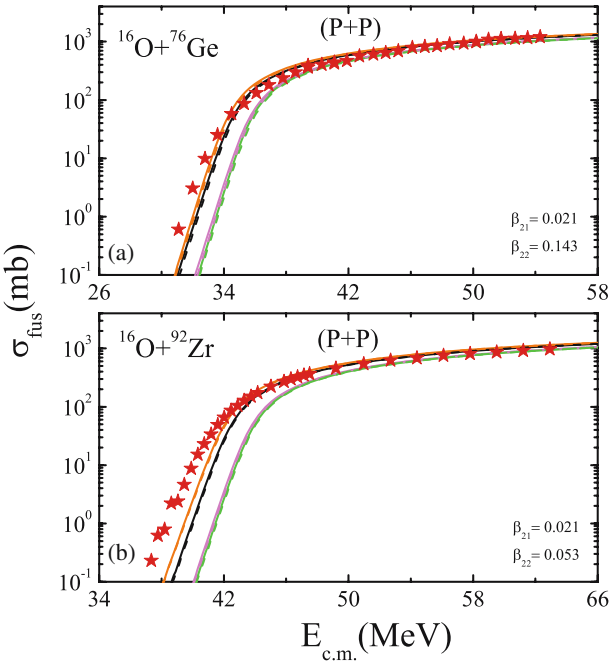

Figure 5. Same as figure 2, but for (**a**) ^{16}O+^{76}Ge and (**b**) ^{16}O+^{92}Zr reactions. In both (**a**) and (**b**), projectile and target are prolate-deformed. The experimental data for these reactions are taken from Aguilera *et al* [22] and Newton *et al* [23], respectively.

4. Summary

In this paper, the role of deformed Coulomb potential on fusion probabilities was studied using Skyrme energy density formalism. It was found that the depth of the fusion pocket is modified on adding deformed Coulomb potential of the colliding nuclei. The fusion pocket becomes deeper for the cases of S+O, O+O compared to spherical–spherical case and shallower for the cases of S+P, P+P compared to spherical ones. Also, a universal trend was seen, i.e., fusion probability increases for S+O, O+O combinations (this change is too small to explain the fusion enhancement at sub-barrier energies), and decreases for S+P and P+P combinations. Hence the deformed Coulomb potential affects the fusion barriers as well as fusion probabilities of the colliding nuclei, but the effect is marginal.

Acknowledgements

The financial support from Council of Scientific and Industrial Research (CSIR), New Delhi, is acknowledged. The authors are thankful to Professor Rajeev K Puri for valuable suggestions and fruitful discussions on the present work.

References

[1] Y K Vermani and R K Puri, *Eur. Phys. Lett.* **85**, 62001 (2009); *ibid*., *J. Phys. G: Nucl. Part. Phys.* **36**, 105103 (2009)
Y K Vermani, S Goyal and R K Puri, *Phys. Rev. C* **79**, 064613 (2009)
Y K Vermani *et al*, *J. Phys. G: Nucl. Part. Phys.* **37**, 015105 (2010)

[2] S Kaur and R K Puri, *Phys. Rev. C* **87**, 014620 (2013)

[3] S Gautam *et al*, *Phys. Rev. C* **85**, 067601 (2012); *ibid.*, **86**, 034607 (2012)
R Bansal *et al*, *Phys. Rev. C* **87**, 061602(R) (2013)

[4] I Dutt and R K Puri, *Phys. Rev. C* **81**, 044615 (2010); *ibid.*, **81**, 047601 (2010); *ibid.*, **81**, 064608 (2010); *ibid.*, **81**, 064609 (2010) and references therein

[5] R K Puri and R K Gupta, *J. Phys. G: Nucl. Part. Phys.* **17**, 1933 (1991); *ibid*., **18**, 903 (1992); *ibid*., *Phys. Rev. C* **45**, 1837 (1992)
M K Sharma *et al*, *Eur. Phys. J. A* **2**, 69 (1998)
R K Puri and N K Dhiman, *Eur. Phys. J. A* **23**, 429 (2005); *ibid*., *Acta. Phys. Pol. B* **37**, 1855 (2006); *ibid.,* **38**, 2133 (2007)

[6] R K Puri and R K Gupta, *Int. J. Mod. Phys. E* **1**, 269 (1992)

[7] T H R Skyrme, *Phil. Mag.* **1**, 1043 (1956); *ibid*., *Nucl. Phys. A* **9**, 615 (1959)

[8] C K Phookan and K Kalita, *Nucl. Phys. A* **899**, 29 (2013)
V V Sargsyan *et al*, *Phys. Rev. C* **84**, 064614 (2011); *ibid.*, **85**, 017603 (2012); *ibid.*, **85**, 037602 (2012)
Z Gao-Long, L Xias-Yun and L Zu-Hua, *Chin. Phys. Lett* **25**, 1247 (2008)
B V Carlson, L C Chamon and L R Gasques, *Phys. Rev. C* **70**, 057602 (2004)

[9] M Manhas *et al*, *Phys. Rev. C* **74**, 034603 (2006)

[10] D Vautherian and D M Brink, *Phys. Rev. C* **5**, 626 (1972)

[11] J Blocki, J Randrup, W J Swiatecki and C F Tsang, *Ann. Phys.* (*NY*) **105**, 427 (1977)

[12] V Yu Denisov and N A Pilipenko, *Phys. Rev. C* **76**, 014602 (2007); *ibid*., *Ukr. J. Phys.* **53**, 845 (2008); *ibid*., *Phys. Atm. Nuclei* **73**, 1152 (2010)

[13] P Moller *et al*, *Atom. Nucl. Data Tables* **59**, 185 (1995)

[14] C Y Wong, *Phys. Rev. Lett.* **31**, 766 (1973)

[15] H Bethe, *Phys. Rev.* **51**, 1125 (1940)

[16] D H Hill and J A Wheeler, *Phys. Rev.* **89**, 1102 (1953)

[17] A Morsad *et al*, *Phys. Rev. C* **41**, 988 (1990)

[18] A M Stefanini *et al*, *Nucl. Phys. A* **456**, 509 (1986)

[19] M Beckerman *et al*, *Phys. Rev. C* **25**, 837 (1982)

[20] H Timmers *et al*, *Nucl. Phys. A* **633**, 421 (1998)

[21] K Siwek-Wilczyńska and J Wilczyński, *Phys. Rev. C* **69**, 024611 (2004)

[22] E F Aguilera, J J Kolata and R J Tighe, *Phys. Rev. C* **52**, 3103 (1995)

[23] J O Newton *et al*, *Phys. Rev. C* **64**, 064608 (2001)